Stability analysis of weak rural electrification microgrids with droop-controlled rotational and electronic distributed generators

Zhao Wang and Michael Lemmon
Department of Electrical Engineering
University of Notre Dame
Notre Dame, IN 46556
Email: zwang6@nd.edu and lemmon@nd.edu

***Abstract*—Droop-controlled distributed generation (DG) units are widely used in microgrids for rural electrification applications. In these microgrids, power quality is vulnerable to voltage and frequency instabilities due to limited generation capacities of DG units. More importantly, droop-controlled rotational and electronic DG units have different frequency dynamics, making a comprehensive stability analysis difficult. By introducing an equivalence between rotational and electronic generators, voltage stability and frequency synchronization conditions are derived as inequality constraints on network parameters, load levels and generator control commands. Satisfying these conditions ensures asymptotic voltage stability and frequency synchronization in a rural electrification microgrid. Moreover, these stability conditions help to economically expand isolated microgrids to a power distribution network that supplies reliable power services.**

***Index Terms*—Voltage stability, frequency synchronization, droop-controlled generator, rural electrification.**

I. INTRODUCTION

In rural electrification projects, distributed generators are usually organized in a microgrid to improve power quality and reliability [1]. Power quality, which is measured in voltage magnitudes and network frequencies, is vulnerable in these weak microgrids due to DG units' limited generation capacities. In addition, because of coupled voltage and frequency dynamics in weak networks, it is difficult to guarantee voltage stability and frequency synchronization simultaneously. More importantly, DG units based on rotational generators and electronic inverters have different frequency dynamics, making a comprehensive stability analysis even more challenging.

Stability analysis of power networks is a long-treated topic. Lyapuove-based transient stability analysis has been studied since the 1970s. In the work by Pai [2], a Lyapunov function was constructed for a lossless single-machine system. More general cases of lossless multi-machine power networks were treated in [3][4]. To make transient stability analyses more realistic, the lossless network assumption was relaxed in [5]. Moreover, voltage dynamics were included in the form of field flux decays [6] and automatic voltage regulators [7]. These early research efforts focused on finding the best Lyapunov function and the critical energy associated to a particular fault [8]. Nevertheless, transient stability analysis did not provide explicit stability conditions for weak networks. To analyze weak power networks, prior research [9][10][11] checked small-signal stability through eigenvalues of linearized network models, but linearized analysis only applied to a small neighborhood of the operating point and are difficult to use.

In addition, droop-controlled rotational and electronic generators have different frequency dynamics, making a comprehensive stability analysis complicated. Different from rotational generators with significant inertia, electronic inverters have fast dynamics [12]. Based on nonlinear oscillator synchronization analysis in [13], an equivalence was pointed out in [14] between a rotational generator and an electronic generator with low-pass filters. However, all generators in [14] had identical parameters, unrealistic in rural electrification microgrids.

A comprehensive stability analysis solves these problems by deriving voltage and frequency stability conditions for weak microgrids with both rotational and electronic generators. Coupled dynamics in weak networks are taken into account, together with different dynamics of rotational and electronic generators. The derived conditions are inequality constraints on network parameters, load levels, and generator control commands. These stability conditions also guide economically expanding isolated microgrids to a reliable power network.

The remainder of this paper is organized as follows. Section II reviews background and notations used in this paper. Section III introduces a weak network model and the equivalence between rotational and electronic generators. Section IV presents sufficient conditions that ensure asymptotic voltage stability and frequency synchronization. Section V demonstrates simulation results showing that the stability conditions help to economically expand isolated microgrids into a reliable network. Section VI provides concluding remarks of weak microgrid stability analysis.

II. BACKGROUND AND NOTATIONS

This section reviews the power flow relationship between buses and a general load model. Three-phase balanced operation and per-unit (p.u.) normalization are basic assumptions throughout this paper. Under these assumptions, admittance matrix $\boldsymbol{Y}_{n\times n}$ of an n-bus network is defined as a symmetric complex matrix [15]. The admittance matrix $\boldsymbol{Y}_{n\times n}$ is also expressed as $\boldsymbol{Y}_{n\times n} = \boldsymbol{G}_{n\times n} + j\boldsymbol{B}_{n\times n}$, where $\boldsymbol{G}_{n\times n}$ is conductance matrix and $\boldsymbol{B}_{n\times n}$ is susceptance matrix. Although

The authors gratefully acknowledge the partial financial support of Notre Dames Environmental Change Initiative and the National Science Foundation (CNS-1239222).

978-1-4673-8040-9/15/$31.00 ©2015 IEEE

balanced operation is assumed, unbalanced situations can be analyzed by decomposing unbalanced vectors into three sets of symmetrical components and treating each set respectively.

Each bus connects a generator and a load: $P_{gen,i}$ and $Q_{gen,i}$ are generated power; $P_{load,i}$ and $Q_{load,i}$ denote real and reactive loads. At any bus i, E_i is voltage magnitude and δ_i is phase angle; P_i and Q_i are injected power. Injected power flows at bus i are expressed as $P_i = P_{gen,i} - P_{load,i}$ and $Q_i = Q_{gen,i} - Q_{load,i}$. A pure load bus j without any generator has $P_j + P_{load,j} = 0$ and $Q_j + Q_{load,j} = 0$.

Power flows between buses are expressed in power balance relationships, where P_i and Q_i at bus i are expressed in functions as follows,

$$P_i = \sum_{j=1}^{n} E_i E_j (G_{ij}\cos(\delta_i - \delta_j) + B_{ij}\sin(\delta_i - \delta_j)), \quad (1)$$

$$Q_i = \sum_{j=1}^{n} E_i E_j (G_{ij}\sin(\delta_i - \delta_j) - B_{ij}\cos(\delta_i - \delta_j)). \quad (2)$$

In equations (1) and (2), real and reactive power values are coupled through sinusoidal functions.

Weak network scenarios [16] initially emerge from connecting wind generators through long feeders and transferring large power flows. Weak networks also exist in rural electrification projects [17] where DG units are used to supply electricity to remote villages. Weak networks are characterized based on power flow stress in the sense of short-circuit ratio (SCR) [16]. SCR is the ratio between the short circuit power at a generator bus and the maximum apparent power of this generator. A typical power distribution network's SCR is around 1000, while a network with SCR around 150 is considered *weak*.

A rural electrification microgrid connects various types of loads that are represented using a ZIP model [18]. The ZIP model is a polynomial load model that combines constant-impedance (Z), constant-current (I) and constant-power (P) components. The real and reactive power loads at bus i are defined as functions of voltage magnitude E_i in p.u. as

$$P_{load,i} = E_i^2 P_{load,a,i} + E_i P_{load,b,i} + P_{load,c,i},$$
$$Q_{load,i} = E_i^2 Q_{load,a,i} + E_i Q_{load,b,i} + Q_{load,c,i}.$$

In the equations above, $P_{load,a,i}$ and $Q_{load,a,i}$ are nominal constant-impedance loads, e.g. incandescent light bulbs and resistance heaters; $P_{load,b,i}$ and $Q_{load,b,i}$ are nominal constant-current loads, usually representing active motor controllers; $P_{load,c,i}$ and $Q_{load,c,i}$ are nominal constant-power loads, generally as a result of power control mechanisms. This ZIP load model approximates a variety of loads in a microgrid.

III. System Model

To analyze a rural electrification microgrid with both rotational and electronic generators, an equivalence was introduced between the dynamics of a synchronous generator and a fast inverter with low pass filters [14]. In this paper, an n-bus microgrid is modeled with m electronic generator buses, g rotational generator buses, and l pure load buses.

Electronic generators are managed by a droop controller, such as the CERTS (Consortium for Electric Reliability Technology Solutions) droop-control mechanism [1]. For m electronic generator buses, phase angle and voltage dynamic equations of the ith electronic generator are

$$\dot{\delta}_i = m_{P,i}(P_{ref,i} - P^m_{gen,i}) + \omega_0, \quad (3)$$

$$\dot{E}_i = (E_{ref,i} - E_i) - m_{Q,i} Q^m_{gen,i}, \quad (4)$$

for all $i \in \{1, 2, \ldots, m\}$, where $m_{P,i}$ is droop slope of the P-frequency droop controller; ω_0 is nominal angular frequency; $m_{Q,i}$ is droop slope of the Q-E droop controller. In equations above, $P_{ref,i}$ and $E_{ref,i}$ denote real power and voltage control commands. $P^m_{gen,i}$ and $Q^m_{gen,i}$ are measured powers as feedbacks to the droop controller. Slopes of droop controllers, i.e. $m_{P,i}$ and $m_{Q,i}$, also reflect the real or reactive power capacities of the electronic generator at bus i.

For g rotational generator buses, phase angle dynamic equation of the ith rotational generator is

$$M_i\ddot{\delta}_i + D_i\dot{\delta}_i = P_{ref,i} + D_i\omega_0 - P_{gen,i}, \quad (5)$$

for all $i \in \{m+1, \ldots, m+g\}$, where M_i is the machine's inertia and D_i is the damping ratio at bus i. It is assumed that rotational generators' voltages are managed by excitation systems that have the same droop controller as in equation (4).

As pointed out in [14], phase angle dynamics of a rotational generator are equivalent to dynamics of an electronic generator with low pass filters. These low pass filters are incorporated into droop controllers of electronic generators through power measurements dynamics

$$\tau_{S,i}\dot{P}^m_{gen,i}(t) + P^m_{gen,i}(t) = P_{gen,i}(t), \quad (6)$$

$$\tau_{S,i}\dot{Q}^m_{gen,i}(t) + Q^m_{gen,i}(t) = Q_{gen,i}(t), \quad (7)$$

where $\tau_{S,i}$ is power measurement time costant at bus i, such as 0.01 *sec* in a CERTS droop controller.

Low-pass filters affect both phase angle and voltage dynamics. In phase angle dynamics, the low-pass filters transform equation (3) to

$$\frac{d}{dt}\dot{\delta}_i(t) = -\frac{m_{P,i}}{\tau_{S,i}}(-P^m_{gen,i}(t) + P_{gen,i}(t)),$$
$$= \frac{m_{P,i}}{\tau_{S,i}}(P_{ref,i} - \frac{1}{m_{P,i}}\dot{\delta}_i(t) + \frac{1}{m_{P,i}}\omega_0 - P_{gen,i}(t)).$$

The second-order phase angle dynamic equation is rewritten as $\frac{\tau_{S,i}}{m_{P,i}}\ddot{\delta}_i(t) + \frac{1}{m_{P,i}}\dot{\delta}_i(t) = P_{ref,i} + \frac{1}{m_{P,i}}\omega_0 - P_{gen,i}(t)$, which has the same form as equation (5). In the dynamic equation of phase angle δ_i, reducing the time constant $\tau_{S,i}$ to zero results in changed dynamic behaviors, so that the second-order term $\ddot{\delta}_i$ is kept. Although different generators have the same phase angle dynamics, parameters vary from machine to machine. A rotational generator has large inertia M_i but small damping ratio D_i, while an electronic generator has small inertia $\tau_{S,j}/m_{P,j}$ and damping ratio $1/m_{P,j}$.

In voltage dynamics, including low-pass filters leads to $\tau_{S,i}\ddot{E}_i(t) + (\tau_{S,i} + 1)\dot{E}_i(t) + E_i(t) = E_{ref,i} - m_{Q,i}Q_{gen,i}(t)$.

When time constants $\tau_{S,i}$ are small, for instance 0.01 *sec*, the second-order voltage dynamic equation simplifies to

$$\dot{E}_i(t) = (E_{ref,i} - E_i(t)) - m_{Q,i}Q_{gen,i}(t). \tag{8}$$

Equation (8) is similar to equation (4), but ignores the impact of power measurement dynamics. Phase angle dynamics in equation (5) and voltage dynamics in equation (8) are used for a rural electrification microgrid with distributed generators.

In the n-bus power network, phase angles of the first $(n-1)$ buses are referred to bus n. With phase angle difference $\theta_i = \delta_i - \delta_n$ for all $i \in \{1, 2, \ldots, n-1\}$ with $\theta_n = 0$, a steady state $(\boldsymbol{P}_{ss}, \boldsymbol{Q}_{ss}, \boldsymbol{\theta}_{ss}, \boldsymbol{E}_{ss}, \omega_{ss})$ is a zero point of dynamic equations in equations (5) and (8). To define the power network model, we introduce set point $(\boldsymbol{P}_{set}, \boldsymbol{Q}_{set}, \boldsymbol{\theta}_{set}, \boldsymbol{E}_{set}, \omega_{set})$, which is a steady state. *Assumption* 1 is made for the set point:

Assumption 1: Set point $(\boldsymbol{P}_{set}, \boldsymbol{Q}_{set}, \boldsymbol{\theta}_{set}, \boldsymbol{E}_{set}, \omega_{set})$ is assumed to be an isolated equilibrium point.

A microgrid manager usually determines set point $(\boldsymbol{P}_{set}, \boldsymbol{Q}_{set}, \boldsymbol{\theta}_{set}, \boldsymbol{E}_{set}, \omega_{set})$ by solving an optimal power flow (OPF) problem and designates control commands $E_{ref,i}$ and $P_{ref,i}$ to bus i

$$E_{ref,i} = E_{set,i} + m_{Q,i}(Q_{set,i} + Q_{load,i}(E_{set,i})), \tag{9}$$

$$P_{ref,i} = P_{set,i} + P_{load,i}(E_{set,i}) + D_i(\omega_{set} - \omega_0). \tag{10}$$

With respect to the set point $(\boldsymbol{P}_{set}, \boldsymbol{Q}_{set}, \boldsymbol{\theta}_{set}, \boldsymbol{E}_{set}, \omega_{set})$, a complete system model is used to analyze voltage stability and frequency synchronization. In the n-bus network, for m electronic generator buses and g rotational generator buses, phase angle dynamics are

$$\begin{aligned} M_i\ddot{\delta}_i + D_i\dot{\delta}_i &= P_{ref,i} + D_i\omega_0 - P_{load,i} - P_i, \\ &= P_{sync,i} - \sum_{\substack{j=1 \\ j\neq i}}^{n} E_iE_j\sin(\delta_i - \delta_j + \phi_{ij}), \end{aligned} \tag{11}$$

for all $i \in \{1, 2, \ldots, m+g\}$, where synchronization power is $P_{sync,i} = P_{ref,i} - P_{load,i}(E_i) - E_i^2G_{ii}$ with $\phi_{ij} = \phi_{ji} = \tan^{-1}(G_{ij}/B_{ij}) \in [-\frac{\pi}{2}, 0]$. For voltage stability analysis, error states are defined with respect to the isolated set point for phase angle $\tilde{\theta}_i = \theta_i - \theta_{set,i}$, voltage magnitude $\tilde{E}_i = E_i - E_{set,i}$ and reactive power $\tilde{Q}_i = Q_{set,i} - Q_i$. For the n-bus network, voltage error dynamics model is:

$$\begin{aligned} \dot{\tilde{E}}_i &= (E_{set,i} - E_i) + m_{Q,i}(Q_{gen,set,i} - Q_{gen,i}), \\ &= m_{Q,i}\tilde{Q}_i - \tilde{E}_i - m_{Q,i}[Q_{load,b,i} + (E_i + \tilde{E}_i)Q_{load,a,i}]\tilde{E}_i, \\ &\quad i \in \{1, \ldots, m+g\} \end{aligned} \tag{12}$$

$$\begin{aligned} \tilde{Q}_i &= Q_{load,a,i}\tilde{E}_i^2 + (2Q_{load,a,i}E_{set,i} + Q_{load,b,i})\tilde{E}_i. \\ &\quad i \in \{m+g+1, \ldots, m+g+l\} \end{aligned} \tag{13}$$

Equation (13) is an algebraic relation between voltage magnitude error $\tilde{E}_i$ and reactive power error $\tilde{Q}_i$ at pure load buses, hence voltage dynamics are governed by generator buses.

Based on the model in equations (11) and (12), definitions of frequency synchronization and voltage stability are as follows.

Definition 1: A microgrid has asymptotic frequency stability if there are two open subsets of $\Omega_{\boldsymbol{E},1}, \Omega_{\boldsymbol{\theta},1} \subset \mathbb{R}^n$ containing the origin such that if any $\tilde{\boldsymbol{E}}(0) \in \Omega_{\boldsymbol{E},1}$ and any $\boldsymbol{\theta}(0) \in \Omega_{\boldsymbol{\theta},1}$ then $\lim_{t\to\infty} \dot{\delta}_i(t) = \omega_{set}$.

Definition 2: A microgrid has asymptotic voltage stability if there are two open subsets of $\Omega_{\boldsymbol{E},2}, \Omega_{\boldsymbol{\theta},2} \subset \mathbb{R}^n$ containing the origin such that if any $\tilde{\boldsymbol{E}}(0) \in \Omega_{\boldsymbol{E},2}$ and any $\boldsymbol{\theta}(0) \in \Omega_{\boldsymbol{\theta},2}$ then $\lim_{t\to\infty} \tilde{\boldsymbol{E}}(t) = \boldsymbol{0}$.

IV. Main Result

This section derives sufficient conditions for voltage stability and frequency synchronization in a weak rural electrification microgrid with both rotational and electronic DG units. These stability conditions are in the form of network parameters, loads and generator control commands. As long as these conditions are satisfied, the network states asymptotically converge to the set point $(\boldsymbol{P}_{set}, \boldsymbol{Q}_{set}, \boldsymbol{\theta}_{set}, \boldsymbol{E}_{set}, \omega_{set})$. The stability analysis decomposes into three steps: i) an invariant set phase angle differences is identified in *Lemma* 1; ii) asymptotic stabilities of both phase angle differences and voltages are proven in *Theorem* 3 and 4; iii) a frequency synchronization conclusion is obtained in *Theorem* 5. Voltage control analysis is the same as an earlier paper [19], while frequency synchronization analysis is presented in this section. Frequency synchronization deals with both rotational and electronic DG units, compared to only inverter-based sources in [19]. Due to limited space, detailed proofs are not provided.

Existence of a voltage invariant set $\boldsymbol{\mathcal{I}_E}$ is established for generator voltages in [19]. As voltages are bounded within $\boldsymbol{\mathcal{I}_E}$, a condition is determined for a positive invariant set of phase angles, such that phase angle differences are kept bounded. Drawing upon techniques used in [13][20], the following lemma characterizes a phase angle difference invariant set.

Lemma 1: Assume there exists a voltage invariant set $\boldsymbol{\mathcal{I}_E}$ with $E_{\min}$ and $E_{\max}$. Define $A_1 = nE_{\min}^2 \min_{i\neq j}(|B_{ij}|)$ and $A_2 = \max_{i\neq j}(|P_{sync,i} - P_{sync,j}|) - 2E_{min}^2|G_{ii}|_{min}$ with nonzero B_{ij} and $P_{sync,i} = P_{ref,i} - P_{load,i}(E) - E_i^2G_{ii}$, if

$$A_1\sin(\theta) \geq A_2, \tag{14}$$

then there exists a non-empty set

$$\boldsymbol{\mathcal{I}_\theta} = \{\theta \in \mathbb{R}^m : \max_{i,j}(|\theta_i - \theta_j|) \leq \theta, \theta \in [0, \pi]\},$$

which is positively invariant.

Building upon the two invariant sets $\boldsymbol{\mathcal{I}_E}$ and $\boldsymbol{\mathcal{I}_\theta}$, asymptotic convergence of phase angle differences requires a stricter condition than *Lemma* 1. The following theorem establishes sufficient conditions for phase angle differences convergence.

Theorem 3: Define $A_1 = nE_{\min}^2 \min_{i\neq j}(|B_{ij}|)$ and $A_2 = \max_{i\neq j}(|P_{sync,i} - P_{sync,j}|) - 2E_{min}^2|G_{ii}|_{min}$, with nonzero B_{ij} and $P_{sync,i} = P_{ref,i} - P_{load,i}(E) - E_i^2G_{ii}$. Under conditions in *Lemma* 1, if

$$A_1\sin(\pi/2 - \alpha_{\max}) \geq A_2, \tag{15}$$

where $\alpha_{\max} = \max_{i\neq j}(\tan^{-1}(\frac{-G_{ij}}{B_{ij}}))$, then there is $\lim_{t\to\infty}\theta_i(t) = \theta_{set,i}$ for each $i \in \{1, 2, \ldots, n\}$.

As long as the phase angle differences asymptotically converge to set point $\boldsymbol{\theta}_{set}$, the following theorem establishes asymptotic voltage stability.

Theorem 4: Assume that conditions in *Lemma* 1 and *Theorem* 3 hold, then phase angle difference $\boldsymbol{\theta}$ converges to $\boldsymbol{\theta}_{set}$ and voltage magnitudes are within invariant set $\boldsymbol{\mathcal{I}_E}$. Define $B_1 = \min_i(\frac{1+Q_{load,b,i}}{m_{Q,i}} + (E_{equ,i} + E_i)Q_{load,a,i})$ and $B_2 = \max\{\sqrt{\lambda} : \lambda \text{ is an eigenvalue of } (\partial \boldsymbol{Q}/\partial \boldsymbol{E})^*(\partial \boldsymbol{Q}/\partial \boldsymbol{E})\}$. If

$$B_1 > B_2, \tag{16}$$

then vector $\{E_i\}$ asymptotically converges to $\{E_{set,i}\}$.

Since conditions in *Lemma* 1, as well as *Theorem* 3 and 4 are all satisfied, phase angle differences $\boldsymbol{\theta}$ converges to $\boldsymbol{\theta}_{set}$ and voltage magnitudes $\boldsymbol{E}$ converges to $\boldsymbol{E}_{set}$. Frequency synchronization to ω_{set} is established in the following theorem.

Theorem 5: Assume that conditions in *Lemma* 1, *Theorem* 3 and *Theorem* 4 hold, then the network frequency asymptotically converges to the set point ω_{set}, i.e. $\lim_{t\to\infty} \dot{\delta}_1(t) = \ldots = \lim_{t\to\infty} \dot{\delta}_n(t) = \omega_{set}$.

V. Simulation Experiments

Stability conditions ensure asymptotic voltage stability and frequency synchronization for microgrids in our rural electrification project in Africa [17]. These conditions also help to economically expand isolated microgrids into a reliable small-scale distribution network by choosing appropriate cables. System responses are simulated as load increases, which are common events in these microgrids. When generators can barely supply the total load, the stability conditions derived in Section IV predict voltage and frequency instabilities. To ensure power service reliability, one should choose thick cables that satisfy all stability conditions. The decisions, however, are also sensitive to construction costs of long cables. Simulation shows that, using the stability conditions, an economical cable choice is made that guarantees power service reliability.

To provide reliable electricity to schools, hybrid microgrids have been installed with diesel generators and solar panels, as shown in plot (a) of Figure 1. These single-phase microgrids operate at 230V and 50Hz. DG units include a 6.5kW diesel genset, a 28.8kWh battery, and a 1250W solar panel. Three load buses include an office (550W), an activity center (570W), and several dorms (240W). All buses are connected using No.6 AWG cables. As shown in Table I, No.6 AWG cables have a power flow limit of 12.65kVA so that are sufficient to supply a total load of 1.36kW. Another hybrid microgrid has the same generators but a total load of 2.12kW.

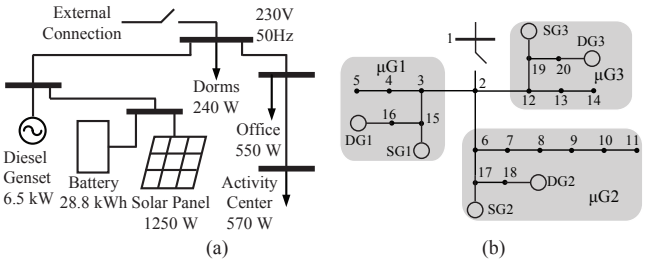

Fig. 1. (a) Hybrid microgrid in the African rural electrification project; (b) simulation model of the expanded rural electrification network.

In the near future, these microgrids are expected to provide power services to more customers. Load levels in simulations are assumed to double the current values and isolated microgrids are connected together. As a result of the interconnection, power generation and consumption within a local microgrid can be balanced by other microgrids with extra capacities. A fundamental problem is whether the expansion has an adverse impact on network stability.

Microgrid interconnection is shown in plot (b) of Figure 1. Each microgrid connects to bus 2 through a *one-mile* feeder, using four types of cables, i.e. No.6, No.4, No.2, and No.00 AWG wires. These cables are sufficient to handle power flows in the expanded network so that cable choice is made based on stability and cost. For instance, No.00 AWG cables are thick to ensure stability yet cost eight times of No.6 AWG cables.

TABLE I
Cable Parameters and Estimated Costs

AWG Cable	$Z\ (R + jX)$ $(\Omega/mile)$	Diameter (inch)	Power Limit (kVA)	Cost $(\$/mile)$
No.00	$0.4751 + j0.2973$	0.3648	33.35	$21,000$
No.2	$0.7982 + j0.4463$	0.2576	21.85	$10,500$
No.4	$1.2936 + j0.6713$	0.2043	16.10	$5,800$
No.6	$2.0952 + j0.7758$	0.1620	12.65	$2,500$

Set points used in simulation tests are obtained by solving an optimal power flow (OPF) problem. Since the total load is well below local generators' capacity within a microgrid, the optimal strategy is to supply all loads by local generators to minimize power loss along the long feeders. The equilibrium point has a frequency of 50 Hz, and voltage magnitudes are between 0.97 p.u. and 1.03 p.u.. The simulation process begins at 1.0 p.u. voltage magnitudes with zero power exchanges and converges to the set point within five seconds. After states converge, a step load increase happens in $\mu G1$ at $t = 25s$ and the voltage responses vary by cable types. In this situation, the load increases from 2.72kW to 13.6kW due to unexpected loads that are brought online for a short time, such as water pumps and air conditioners. These additional loads place a large burden on feeders connecting the microgrids and result in voltage collapses when thin cables are used.

To ensure network stability under step load increases, the condition in *Lemma* 1 is examined for all four types of cables. The condition $A_1 \sin\theta \geq A_2$ must be satisfied to ensure the existence of a phase angle invariant set $\boldsymbol{\mathcal{I}_\theta}$. Network expansion with No.00 AWG cables leads to $(A_1, A_2) = (955.8, 432.18)$, the condition in equation (14) is satisfied. (A_1, A_2) in the case with No.6 AWG cables is $(157.32, 431.72)$, which violates the stability condition. It is then reasonable to use cables with the smallest A_1 that satisfies $A_1 \geq A_2$. Possible choices are No.2 and No.4 AWG cables, whose values of (A_1, A_2) are $(539.53, 432.43)$ and $(319.77, 432.07)$, respectively. *The expanded network connected with No.*2 *AWG cables should be stable, while the one with No.*4 *AWG cables may experience voltage and frequency instability.* As demonstrated in simulations, the occurrence of instability matches predictions made by the stability condition in *Lemma* 1.

Simulation examines frequency and voltage responses to the step load increases using No.2 and No.4 AWG cables.

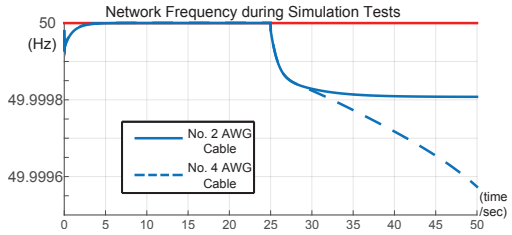

Fig. 2. Frequency responses showing stability with No.2 AWG cables and instability with No.4 AWG cables.

As shown in Figure 2, frequency converges to nominal 50Hz within five seconds of simulation for both cable types. After step load increases, frequency continues to drop in the network with No.4 AWG cables, but stabilizes with No.2 AWG cables in about ten seconds. Similarly, voltage magnitudes in $\mu G1$ are compared in Figure 3.

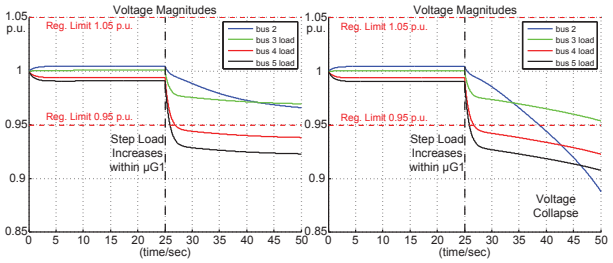

Fig. 3. Voltage responses to load step increases in $\mu G1$ with (Left) No.2 AWG cables and (Right) No.4 AWG cables.

The left plot of Figure 3 shows voltage convergence within five seconds after the step load increase, showing stability with No.2 AWG cables. Voltage magnitudes at bus 2 and 3 stay above 0.96 p.u., satisfying voltage regulation rules. Bus 4 and 5, at the end of $\mu G1$'s feeder line, have their voltages around 0.92 p.u., but the power quality is still acceptable. The right plot of Figure 3 shows voltage collapse in the network with No.4 AWG cables, as *predicted by the stability conditions*. The voltage at bus 2 continues to drop and that might trigger protection mechanisms and cause power service disruption. As a result, the No.2 AWG cables are our choices to reduce construction cost while ensuring stability under step load increases. Compared with No.00 AWG cables, No.2 AWG cables have a similar performance, yet reduce the cost by half.

Satisfying stability conditions ensures asymptotic voltage stability and frequency synchronization of weak rural electrification microgrids coupled with both rotational and electronic DG units. The stability conditions help to expand isolated microgrids into a reliable power network. In conclusion, thick cables should be used to ensure stability, even though their power ratings are higher than microgrid generation capacity.

VI. Summary

Asymptotic stability conditions are derived for *weak* rural electrification microgrids with both rotational and electronic DG units. Used as constraints in OPF problems, these conditions ensure network states asymptotically converge to a set point. Furthermore, these stability conditions provide a guidance in connecting multiple isolated microgrids in our rural electrification project in Africa. Simulation demonstrates that the stability conditions help make an economical cable choice to expand microgrids to a reliable network.

References

[1] R. Lasseter, "Smart distribution: Coupled microgrids," *Proceedings of the IEEE*, vol. 99, no. 6, pp. 1074–1082, 2011.

[2] M. Pai, M. A. Mohan, and J. G. Rao, "Power system transient stability: Regions using popov's method," *Power Apparatus and Systems, IEEE Transactions on*, no. 5, pp. 788–794, 1970.

[3] J. Willems and J. Willems, "The application of lyapunov methods to the computation of transient stability regions for multimachine power systems," *Power Apparatus and Systems, IEEE Transactions on*, no. 5, pp. 795–801, 1970.

[4] E. Carton and M. Ribbens-Pavella, "Lyapunov methods applied to multimachine transient stability with variable inertia coefficients," in *Proceedings of the Institution of Electrical Engineers*, vol. 118, no. 11. IET, 1971, pp. 1601–1606.

[5] T. Athay, R. Podmore, and S. Virmani, "A practical method for the direct analysis of transient stability," *Power Apparatus and Systems, IEEE Transactions on*, no. 2, pp. 573–584, 1979.

[6] N. Kakimoto, Y. Ohsawa, and M. Hayashi, "Transient stability analysis of multimachine power system with field flux decays via lyapunov's direct method," *Power Apparatus and Systems, IEEE Transactions on*, no. 5, pp. 1819–1827, 1980.

[7] H. Miyagi and A. R. Bergen, "Stability studies of multimachine power systems with the effects of automatic voltage regulators," *Automatic Control, IEEE Transactions on*, vol. 31, no. 3, pp. 210–215, 1986.

[8] A. Bose, "Application of direct methods to transient stability analysis of power systems," *Power Apparatus and Systems, IEEE Transactions on*, no. 7, pp. 1629–1636, 1984.

[9] N. Martins, "Efficient eigenvalue and frequency response methods applied to power system small-signal stability studies," *Power Systems, IEEE Transactions on*, vol. 1, no. 1, pp. 217–224, 1986.

[10] L. Wang and A. Semlyen, "Application of sparse eigenvalue techniques to the small signal stability analysis of large power systems," in *Power Industry Computer Application Conference, 1989. PICA'89, Conference Papers*. IEEE, 1989, pp. 358–365.

[11] P. Kundur, G. Rogers, D. Wong, L. Wang, and M. Lauby, "A comprehensive computer program package for small signal stability analysis of power systems," *Power Systems, IEEE Transactions on*, vol. 5, no. 4, pp. 1076–1083, 1990.

[12] Z. Miao, A. Domijan, and L. Fan, "Investigation of microgrids with both inverter interfaced and direct ac-connected distributed energy resources," *Power Delivery, IEEE Transactions on*, vol. 26, no. 3, pp. 1634–1642, 2011.

[13] F. Dorfler and F. Bullo, "Synchronization and transient stability in power networks and non-uniform Kuramoto oscillators," vol. 50, no. 3, pp. 1616–1642, 2012.

[14] J. Schiffer, D. Goldin, J. Raisch, and T. Sezi, "Synchronization of droop-controlled microgrids with distributed rotational and electronic generation," *52nd IEEE CDC, Florence, Italy*, 2013.

[15] A. R. Bergen, *Power Systems Analysis, 2/E.* Pearson Education, 2009.

[16] N. P. Strachan and D. Jovcic, "Stability of a variable-speed permanent magnet wind generator with weak ac grids," *Power Delivery, IEEE Transactions on*, vol. 25, no. 4, pp. 2779–2788, 2010.

[17] "Accenture development partnerships assists university of notre dame to build solar power microgrids in uganda for connectivity, electricity, and education for entrepreneurship," Accenture, Tech. Rep., 2013.

[18] "Load representation for dynamic performance analysis," *Power Systems, IEEE Transactions on*, vol. 8, no. 2, pp. 472–482, 1993.

[19] Z. Wang, M. Xia, and M. Lemmon, "Voltage stability of weak power distribution networks with inverter connected sources," in *American Control Conference, Washington DC, USA*, 2013.

[20] F. Dörfler and F. Bullo, "On the critical coupling for kuramoto oscillators," *SIAM Journal on Applied Dynamical Systems*, vol. 10, no. 3, pp. 1070–1099, 2011.